Biosensors and Bioelectronics xxx (xxxx) xxx

Contents lists available at ScienceDirect

Biosensors and Bioelectronics

journal homepage: http://www.elsevier.com/locate/bios

A terahertz metamaterial biosensor for sensitive detection of microRNAs based on gold-nanoparticles and strand displacement amplification

Ke Yang [a,b,1], Jining Li [c,1], Marc Lamy de la Chapelle [a,d], Guorong Huang [a], Yunxia Wang [a], Jinbao Zhang [b], Degang Xu [c], Jianquan Yao [c], Xiang Yang [a,**], Weiling Fu [a,*]

[a] Department of Laboratory Medicine, Southwest Hospital, Third Military Medical University (Army Medical University), Chongqing, 400038, China
[b] Department of Cardiovascular Surgery, General Hospital of Western Theater Command (Chengdu Military General Hospital), Chengdu, 610036, China
[c] Institute of Laser and Opto-electronics, School of Precision Instrument and Opto-electronics Engineering, Tianjin University, Tianjin, 300072, China
[d] Institut des Molécules et Matériaux du Mans (IMMM-UMR CNRS 6283), Université du Mans, Avenue Olivier Messiaen, 72085, Le Mans, France

ARTICLE INFO

Keywords:
Terahertz metamaterials
microRNA-21
Nanoparticles
Strand displacement amplification

ABSTRACT

Terahertz (THz) spectroscopy has drawn great interest for the functional and conformational investigations of nucleic acids, but its intrinsic sensitivity hinders potential bio-sensing applications. Here, a novel THz biosensor was developed for detecting microRNA (miRNA) samples based on metamaterials coupled with nanoparticles and strand displacement amplification (SDA). In this method, the SDA reaction amplifies the target miRNA and generates copious yields of secondary DNA molecules (Trigger DNA), which are subsequently conjugated to metallic nanoparticles that form nanoparticle-Trigger DNA complexes. These complexes produce remarkable frequency shifts of metamaterials when linked to a large refractive index metallic nanoparticle like Au. The dependence of the metamaterial resonance on the nanoparticle diameter and metal type was investigated experimentally and theoretically. Under optimal conditions, the THz metamaterial biosensor presents good detection sensitivity with a limit of detection of 14.54 aM and exhibits a linear response for miRNA-21 at a concentration range from 1 fM to 10 pM. By measuring the miRNA-21 in spiked clinical serum samples, the sample recoveries were determined to be in the range between 90.92% and 107.01%. These findings demonstrate that the novel THz biosensor offers the capability for highly sensitive miRNA detection, with noteworthy potential applications in nucleic acid analysis and cancer diagnosis.

1. Introduction

MicroRNAs (MiRNAs) are considered as a class of potential biomarkers for diagnosis, prognosis, and therapeutic monitoring of various cancers. Because of their sequence homology, short chains, and low abundance, the accurate quantification of miRNAs remains challenging (Kilic et al., 2018). Recently, terahertz (THz) spectroscopy has emerged as a promising new tool in nucleic acid analysis. This frequency range (0.1–10 THz) gives access to the low-frequency vibrational modes (hydrogen bonds, van der Waals, and non-bonded interactions), which coincidentally provides information on the conformation of biomolecules (Yang et al., 2017). THz spectroscopy has been applied to reveal the biological functions of nucleic acids and their profound dynamic motions, including DNA methylation sites (Cheon et al., 2016), RNA dynamics (Niessen et al., 2019), and oligonucleotides mutations (Tang et al., 2015). Because of the size mismatch between nucleic acid molecules and the wavelength of THz radiation (30 μm–3 mm), the best measurement in the free-space time-domain only achieves a sensitivity of micromolar levels (Tang et al., 2015). Therefore, current research in nucleic acid quantitative detection usually includes some molecular amplification method that is coupled with THz spectroscopy. Our previous work demonstrated that THz spectroscopy with sample amplification can detect the DNA fragments as low as 0.06 nM (Yang et al., 2017). Nevertheless, this sensitivity still does not satisfy clinical miRNAs detection requirements because of the extremely low trace levels (approximately 0.6–30 pg/mL) typically found in plasma (Kilic et al., 2018; Xue et al., 2019).

Recently, metamaterials have been applied to improve the sensitivity

* Corresponding author.
** Corresponding author.
E-mail addresses: yangxiang@tmmu.edu.cn (X. Yang), weiling_fu@126.com (W. Fu).
[1] K. Yang and J.-N. Li contributed equally to this work.

https://doi.org/10.1016/j.bios.2020.112874
Received 11 September 2020; Received in revised form 26 November 2020; Accepted 27 November 2020
Available online 1 December 2020

of THz detection. These artificially engineered electromagnetic materials are attractive tools as they offer large Q-factor values, which enhance localized electric fields. As a result, metamaterials are able to probe the alterations of the surrounding electromagnetic environment and are sensitive to extremely small amounts of substances deposited over their surfaces (Xu et al., 2017). Such materials have improved the sensitivity of THz measurements, as observed for the detection of antibiotics (Qin et al., 2016), DNA (Hasebe et al., 2012), and bacteria (Park et al., 2014). Compared to conventional time-domain THz measurements, as little as 0.1 mg/L of the tetracycline hydrochloride has been detected using metamaterials, which is approximately 10^5 times higher than the normal sensitivity (Qin et al., 2016).

Some pioneering studies have demonstrated that combining THz metamaterials with nanomaterials results in further boosting of performance specifications (Xu et al., 2016). Since the resonant frequency shifts of metamaterials increase with the refractive index of substances, the samples binding to high refractive index materials, such as gold nanoparticles (AuNPs), should achieve stronger THz responses (Xu et al., 2016). Of note, 150 pmol of avidin was successful at generating a frequency shift of 2.61 GHz on a metamaterial consisting of square metal patch arrays, whereas a higher frequency shift (3.12 GHz) was obtained using only 10 fmol of AuNPs conjugated avidin. In this case, the LOD of avidin samples achieved femtomole level, showing another 1000-fold improvement over the AuNP free samples (Xu et al., 2016). Although nanomaterials offer huge potential as new sensitivity improvement tools, the mechanisms of enhanced metamaterial response have not been fully elucidated. Moreover, as the particle size and target components of nanoparticles have varied in practical applications, it has become necessary to systematically investigate the effects of nanoparticle geometry and metal type on the sensitivity of THz metamaterial sensing.

In addition to incorporating improved nanomaterials, THz measurements also benefit by combining with nucleic acid amplification strategies, such as strand displacement amplification (SDA). Differing from traditional polymerase chain reaction (PCR), SDA is an isothermal amplification method with the advantages of high efficiency and simplified instrumentation (Yin et al., 2017). In contrast to signal enhancement by nanoparticles, SDA provides additional physical copies of amplified products of the miRNA targets. Target amplification therefore offers additional sensitivity by a gain factor that is dependent upon the length of the reaction time. Moreover, by incorporating target miRNA-specific probes with low hybridization error, SDA also contributes to the elimination of THz assay noise.

Herein, we fabricated a polarization-independent metamaterial consisting of a planar array of four-gap electric split-ring resonators (SRRs). Based on these metamaterial resonators plus signal enhancing nanoparticles, together with SDA methodology, we produced a highly sensitive THz biosensor for detecting miRNA-21. As a prelude to validating the use of these technologies for bio-sensing applications, we experimentally and theoretically investigate the dependence of the metamaterial sensitivity on the nanoparticle diameter and metal type. Based on the signal enhancement obtained from combined SDA and metallic nanoparticles, the THz biosensor presented remarkable sensitivity and specificity for miRNA-21 detection. The validation of measurements was made by measuring miRNA-21 in spiked clinical serum samples. This biosensor scheme exhibited extraordinary sensitivity toward miRNA detection in practical clinical samples and provided a promising sensing platform for nucleic acid analysis and cancer diagnosis.

2. Experimental section

2.1. Reagents and materials

MiRNA and DNA sequences used in this study are given in Table S1. Information regarding reagents is described in the Supporting Information (SI).

2.2. SDA procedure for copying miRNA molecules

Ten microliters of template DNA (100 nM), 10 μL of different concentrations of miRNAs, 2.5 μL of 10 × CutSmart buffer, and 2.5 μL of DEPC-treated water were mixed. The mixed solution was then heated to 95 °C for 5 min and cooled down to 4 °C for 3 min. Subsequently, the mixture was incubated at 25 °C for 40 min to hybridize template DNA and miRNA. After addition of a 25 μL solution consisting 200 U/mL Klenow fragment polymerase, 200 U/mL Nt.*Bsm*AI nicking endonuclease, 800 μM dNTPs, and 1 × CutSmart buffer, the total 50 μL of mixture (SDA reagent solution) was incubated at 37 °C for 2 h to produce Trigger DNA. Finally, the reaction was terminated by heating the mixture at 75 °C for 20 min. To analyze the SDA products, a 12% nondenaturing polyacrylamide gel electrophoresis (PAGE) was carried out. After 20 min of SYBR Green I staining, the gels were scanned using a gel imaging system (GelDoc XR+, Bio-rad, Shanghai, China).

2.3. Conjugation of Trigger DNA to nanoparticles

Nano-probes were first prepared according to the protocol described in the SI. The UV–Visible spectrophotometer was used to characterize the nano-probes (Fig. S1). Subsequently, 400 μL of the nano-probe (50 μg/mL), 50 μL of the SDA reagent solution, and 50 μL of the biotin-probe (100 μM) were mixed. The mixture was incubated at room temperature for 60 min to form the nanoparticle-Trigger DNA complexes. Excess biotin-probe was removed by centrifugation at 13,000 rpm for 20 min. After this, 200 μL of streptavidin-coated magnetic beads (MB, 5 μg/μL) was added to the precipitates in order to capture the nanoparticle-Trigger DNA complexes. After the purification, the complexes were separated from MBs and removed to the supernatant by heating the solution at 95 °C for 15 min. After the magnetic separation, all MBs were removed and the supernatant was transferred to a clean microcentrifuge tube to carry out the THz measurement. Transmission electron microscopy (TEM) and zeta potential measurements were carried out to characterize the nanoparticle-Trigger DNA complexes on MBs.

2.4. Preparation of clinical serum samples

Serum samples were from healthy volunteers at the Southwest Hospital of Army Medical University, and obtained with ethical approval. Serum was diluted to 10% normal with physiological saline solution. Subsequently, a certain amount of synthetic miRNA-21 (10 pM, 1 pM, 100 fM and 10 fM) was spiked in the diluted sera to prepare the miRNA-21 serum samples. Each sample was measured in triplicate, and the measured concentrations were calculated from calibrations using linear regressions to relate frequency shifts to spiked miRNA concentrations. By comparing the measured concentrations to the added concentrations, the recoveries of serum samples were determined.

2.5. Fabrication of THz metamaterials

THz metamaterials were comprised of a planar array of SRRs on high-resistivity silicon substrates. The four-fold rotationally-symmetric unit cells of the SRRs are polarization independent, which is favorable to assure stability and reproducibility. The detailed dimensions of the metamaterial structure are depicted in Fig. S2. Metamaterial chips containing nine square detection areas (1 × 1 cm^2) were fabricated by standard microfabrication techniques. The reusability of metamaterial chips was examined by repeatedly measuring their resonant frequencies after multiple cleanings. The detailed process and results are reported in Table S2. To ensure sample comparability, we suggest that reuse of each chip be limited to 5 cleaning cycles.

2.6. THz metamaterial measurements

THz metamaterial measurements were performed on a commercial

THz time-domain spectroscopy system (TAS7500SP, Advantest Co., Tokyo, Japan). First, THz transmission spectra were recorded for the bare metamaterial (bare MM) in the square detection area. Then 20 μL of the aforementioned nanoparticle-Trigger DNA complexes were dripped on the square detection areas and dried at 50 °C for 20 min. After complete drying, the transmission spectra of the sample were measured. We measured the metamaterial frequency shifts (Δf) by monitoring the relative changes in the resonance peaks of transmission spectra between the sample and bare MM for all samples. A high-resistivity silicon substrate was used as reference. Each sample was repeatedly measured three times.

The degree of interference (DI) was used to evaluate the specificity of the THz metamaterial biosensor, which was calculated using the following equation,

$$DI = \frac{I - B}{T - B} \times 100\% \quad (1)$$

where I, B, and T represent the$\Delta f$of the interfering miRNA, the blank control (DEPC-treated water), and the target miRNA, respectively.

2.7. Finite element method (FEM) simulation

The simulations of the resonance absorbances and the Δf caused by equivalent dielectric films with different refractive indices were performed using the full-wave finite-integration-technology frequency solver based on commercial software (CST MICROWAVE STUDIO). More specific operational details are discussed in the SI.

3. Results and discussion

3.1. Principle of THz metamaterial biosensor for miRNA-21 detection

The principle of the THz metamaterial biosensor for miRNA-21 detection is illustrated in Fig. 1A. The detection process includes three steps:

(i) *SDA procedure for copying miRNA-21 molecules.* The miRNA-21 is first hybridized to the template DNA and triggers a DNA strand extension using Klenow fragment polymerase. After forming a complete double-stranded DNA, the Nt.*Bsm*AI nicking endonuclease cleaves the extended DNA strand. The Klenow fragment subsequently initiates a new round of replication. The first replicated DNA strand is displaced and released. As a result of numerous repetitions of this cycle, copious quantities of Trigger DNA copies are subsequently produced.

(ii) *Conjugation of Trigger DNA to nanoparticles.* Nanoparticles were first modified with the thiol-probe to form the nano-probe. After the SDA process, nano-probes and biotin-probes hybridized with their complementary segments of Trigger DNA chains. The

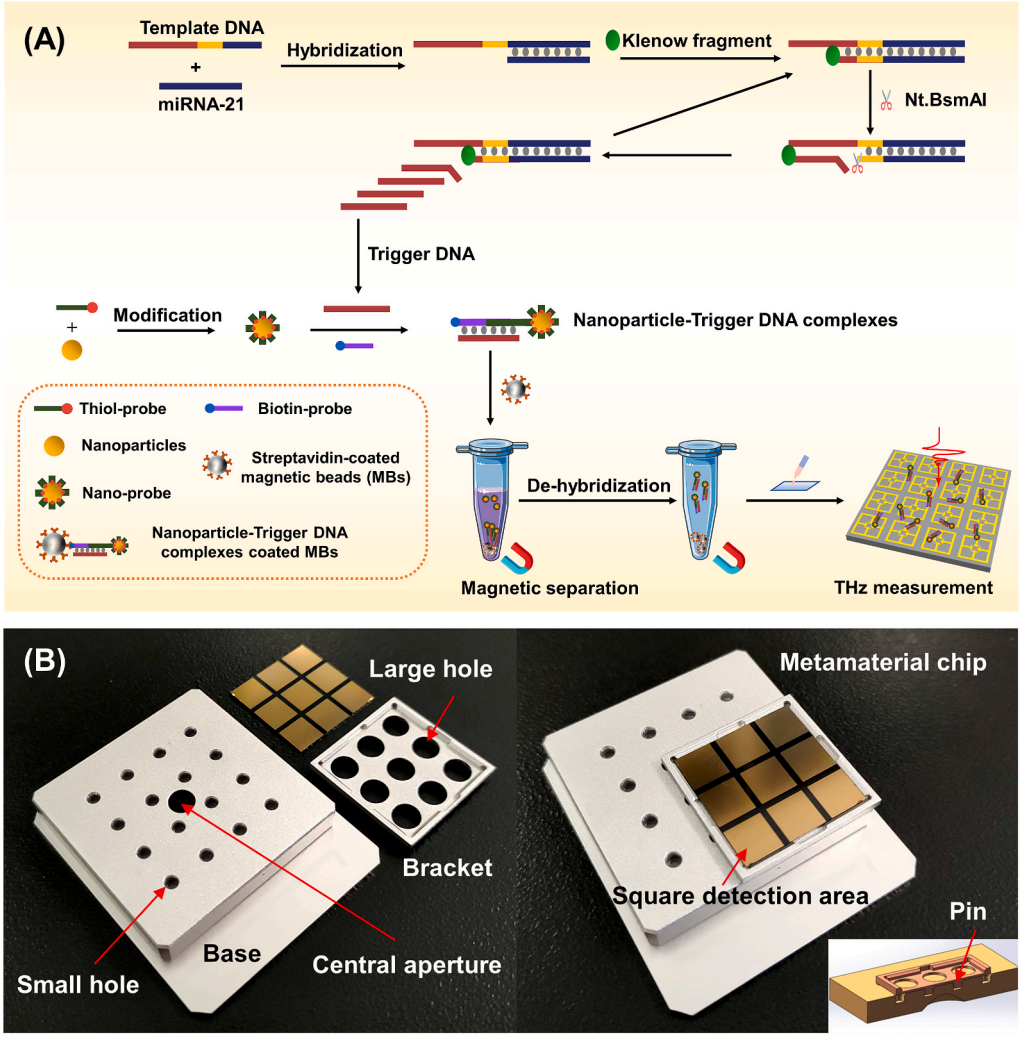

Fig. 1. (A) Schematic description of THz metamaterial biosensor for miRNA detection. (B) Images of the THz metamaterials and chip holder.

resulting structure assembles into a biotinylated nanoparticle-Trigger DNA complex.

(iii) *Purification of complexes and THz metamaterial measurements.* The biotinylated complexes are subsequently captured by binding with streptavidin-coated MBs. After magnetic separation and de-hybridization, the pure nanoparticle-Trigger DNA complexes are isolated and drop cast on the metamaterial surface to perform the THz measurement.

As shown in Fig. 1B, a customized holder was used for the THz measurement. When the chip was centered over the square bracket, its square detection area could be aligned to the large holes. Since detection from each element of the nine element detection areas on the metamaterial chip is independent, nine individual samples can be serially detected by moving the upper bracket into alignment with the square detection area, large hole, and central aperture, without a need for repeated chip washing and drying procedures.

To validate the fidelity of SDA copies, a PAGE analysis was carried out. As shown in Fig. 2A, the bright band in lane 3 migrated at a slower rate than the bands in lane 1 and lane 2, consistent with the effective hybridization of miRNA-21 to template DNA. In addition, the lower band in lane 4, representing the SDA products, nearly matched the band in lane 5 (pure synthetic Trigger DNA). This data demonstrates the generation of Trigger DNA sequences in the SDA products. To further verify if the nanoparticle-Trigger DNA complexes were produced, AuNPs with an average diameter of 50 nm were selected as a pre-tested material for conjugation with the Trigger DNA (Fig. 2B). The nano-probe in Fig. 2C displays a measurable redshift of 5 nm in the UV–Visible spectrum compared with the raw AuNPs, demonstrating grafting of the thiol-probe on AuNPs through the S–Au bond (Li et al., 2018).

TEM and zeta potential measurements were then carried out to characterize the nanoparticle-Trigger DNA complexes on MB carriers (SDA-MBs). As shown in Fig. 2D and E, numerous AuNPs were localized on the surface of the SDA-MBs, while no AuNPs were observed to decorate the blank-MBs. This result agrees with previous TEM studies on the conjugation of probe-functionalized AuNPs with MBs (Tang et al., 2018). In addition, SDA-MBs exhibited a lower zeta potential (-32.00 ± 0.36 mV) than blank-MBs (-28.97 ± 0.17 mV), which also indicates the immobilization of nanoparticle-Trigger DNA complexes on MBs (Fig. 2F).

3.2. Enhancement of THz sensitivity using nanoparticles

The effects of nanoparticle diameter and metal type on metamaterial sensing were investigated to understand what role they play in signal enhancement. AuNPs and AgNPs having average diameters of 20 nm, 50 nm, or 100 nm were conjugated to Trigger DNA to form six types of nanoparticle-Trigger DNA complexes. As shown in Fig. 3A and B, AuNP-Trigger DNA complexes generated larger frequency shifts, Δf, than AgNP-Trigger DNA complexes for all three diameters. We determined that 50 nm nanoparticle-Trigger DNA complexes produced greater Δf than these other diameters. The Δf of these metamaterials can be understood using the following equation (Park et al., 2015),

$$\frac{\Delta f}{f_0} = \frac{\alpha N_s (n_s^2 - n_{air}^2)}{n_0^2}. \quad (2)$$

Here, α is the coefficient that is associated with the sample volume fraction, N_s represents the packing density of sample, and n_s, n_{airs}, and n_0 represent the refractive index of sample, air, and bare MM, respectively. Although there may be a fluctuation in the local α or N_s on each unit of the metamaterial array, we observed that the ensemble average of Δf originating from more than 2000 metamaterial units was located in the focused THz spot (approximately 15 mm^2) during each measurement (Park et al., 2015). Thus, AuNPs and AgNPs can be regarded as having the same α and N_s in metamaterials under the same conditions of particle diameters and concentrations. According to this equation, the samples with higher refractive index should generate greaterΔf. To verify this hypothesis, we utilized finite element modeling (FEM) to simulate the Δf generated by dielectric films of equivalent thicknesses but different refractive indices. As shown in Fig. 3C, with the increase of the refractive indices, the resonant frequency exhibited well-characterized shifts towards low frequency, verifying that higher refractive index films on metamaterials exhibit greater values of Δf. This simulation corresponds well with the experimental data illustrated in Fig. 3A. Therefore, the larger Δf seen for AuNPs-Trigger DNA complexes may be attributed to

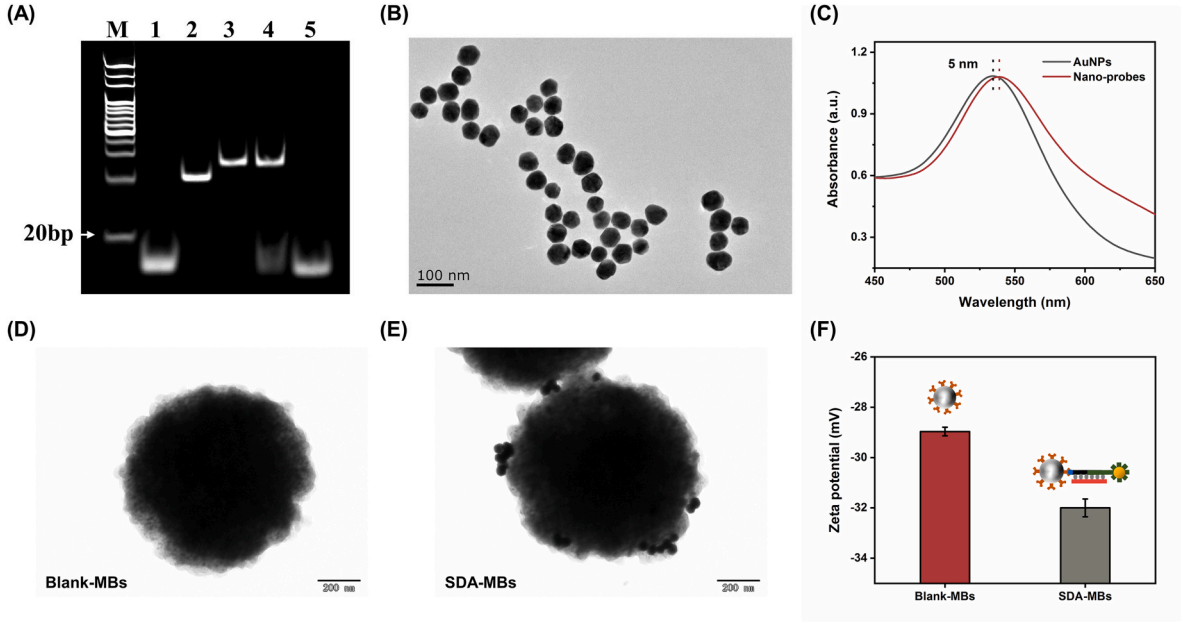

Fig. 2. (A) PAGE analysis of SDA products. Lanes M, 1, 2, 3, 4, and 5 represent the 500 bp DNA ladder marker, miRNA-21, template DNA, hybridization products, SDA products, and pure synthetic Trigger DNA, respectively. One μM of each sequence was used for better illustration. (B) TEM image of 50 nm AuNPs. (C) UV–Visible absorbance spectra of 50 nm AuNPs and nano-probes. (D) TEM image of blank-MBs. (E) TEM image of nanoparticle-Trigger DNA complexes coated MBs (SDA-MBs). (F) Zeta potential of blank-MBs and SDA-MBs. Error bars indicate the SD ($n = 3$).

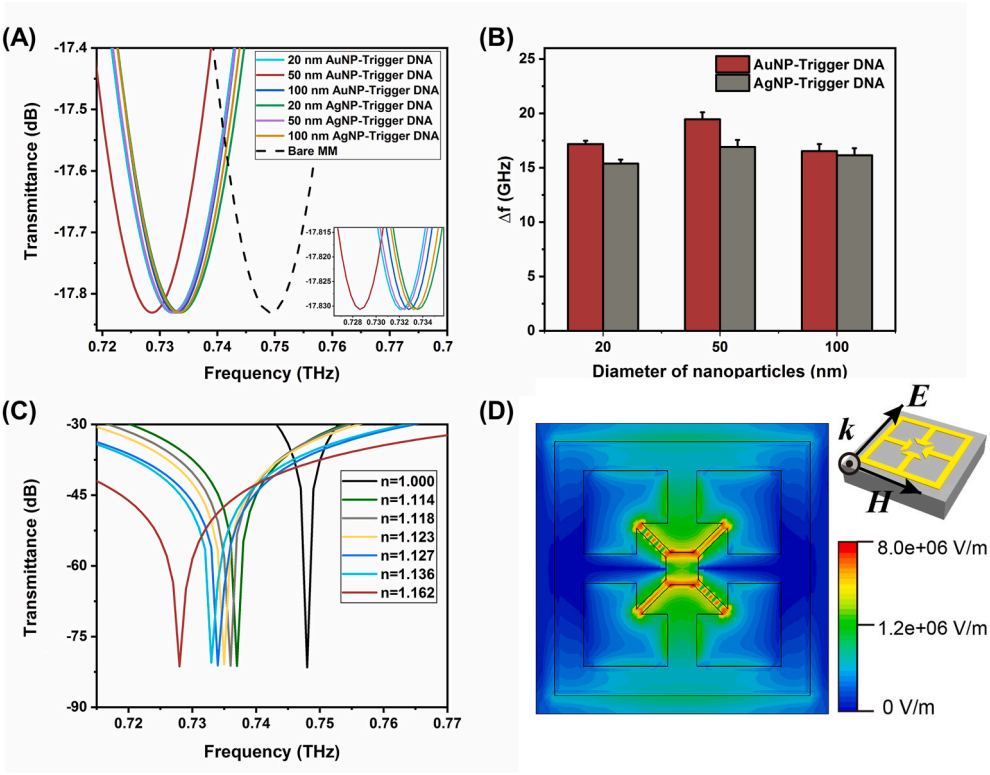

Fig. 3. (A) Normalized THz transmission spectra of six nanoparticle-Trigger DNA complexes and bare metamaterial. Inset graph magnifies the signal from 726.4 to 735.8 GHz. (B) Metamaterial frequency shifts (Δf) of six nanoparticles-Trigger DNA complexes. (C) Simulations of transmission spectra of the metamaterial coated with equivalent dielectric films of different refractive indices. (D) Electric field distribution at the resonant frequency. Error bars indicate the SD ($n = 3$).

the higher refractive index of gold (1.812 at 1 THz) over silver (1.496 at 1 THz) (Lynch and Hunter 1997).

The influence of nanoparticle diameter on Δf is more complex than the influence of element exchange from Ag to Au metal. A previous yeast film detection using metamaterial demonstrated that Δf increases with the increasing thickness of the sample film on the metamaterial surface (Park et al., 2014). The nanoparticle-Trigger DNA complexes can be regarded as a film of the isotropic medium according to effective medium theory. In this case, an increase in nanoparticle diameter is equivalent to a greater thickness of sample on metamaterials (Barrera et al., 1993). As a result, 50 nm nanoparticle-Trigger DNA complexes exhibit greater Δf than 20 nm nanoparticle-Trigger DNA complexes, as shown in Fig. 3A and B. Based on this explanation, the theoretically greatest Δf should be seen for the case of 100 nm nanoparticle-Trigger DNA complexes as opposed to 50 nm complexes. However, as shown in Fig. 3D, a strong electric field is observed only in the central four gaps formed by metal strips in the simulation. Thus, the maximal Δfoccurs when the targets are located inside the metamaterial gap areas. This phenomenon has also been observed in the simulated results of other groups (Park et al., 2015; Xu et al., 2017). Compared to other sizes, 100 nm nanoparticles lack adequate dispersion in the maximum field gaps and are frequently found to form aggregates that are too large to fit inside the gap. This disrupts their packing in the sensing area. Although 100 nm AuNPs-Trigger DNA complexes may contain more Trigger DNA due to the larger surface areas for DNA hybridization, we surmise that the packing of AuNPs have a much more pronounced influence on Δf than the presence of surface-coated DNA molecules. This arises because of the much greater refractive index of the metal than DNA. Therefore, 50 nm AuNPs were ultimately selected as the optimal nanoparticle size for signal enhancement, because of the more favorable combination of size, packing density, and high refractive index.

Fig. 4A and B shows the THz transmission spectra and the Δf measurements of miRNA-21 (100 fM), Trigger DNA, and 50 nm AuNP-Trigger DNA complexes. After the SDA process, Trigger DNA generated greater Δf than miRNA-21. With the introduction of AuNPs, the Δf increases remarkably compared to that of Trigger DNA or miRNA-21. This result illustrates the magnitude of signal enhancement conferred by AuNPs on the measurement of THz metamaterial resonances, as well as the feasibility of using the developed SDA molecule copying strategy to complement the other enhancements for detecting miRNA-21.

3.3. Optimization of experimental conditions

Several experimental parameters were optimized, including the Klenow fragment polymerase concentration, Nt.*Bsm*AI nicking endonuclease concentration, SDA reaction time, and nano-probe concentration. As shown in Fig. S3A, the Δf increased gradually with the increasing Klenow fragment polymerase concentration from 50 to 200 U/mL. Δf remained at a relatively constant level after further increasing the polymerase concentration. Thus, 200 U/mL was selected as the optimal concentration. The effect of the Nt.*Bsm*AI nicking endonuclease concentration on maximizing Δf was also investigated using the same approach (Fig. S3B). The optimal concentration was determined to be 200 U/mL. In addition to the enzyme concentrations, the SDA reaction time required to produce the greatest frequency shifts was determined to be 2 h (Fig. S3C). Finally, the effects of nano-probe concentration on Δf was investigated. As shown in Fig. S3D and 50 μg/mL of nano-probe produced the greatest Δf in the concentration range from 10 to 90 μg/mL.

3.4. Sensitivity of THz metamaterial biosensor for miRNA-21 detection

The THz metamaterial biosensor was evaluated for its sensitivity to detect miRNA-21 under the above optimal experimental conditions. As shown in Fig. 5, Δf increased with increasing miRNA-21 concentration from 10 aM to 100 pM. In addition, a good linear relationship could be

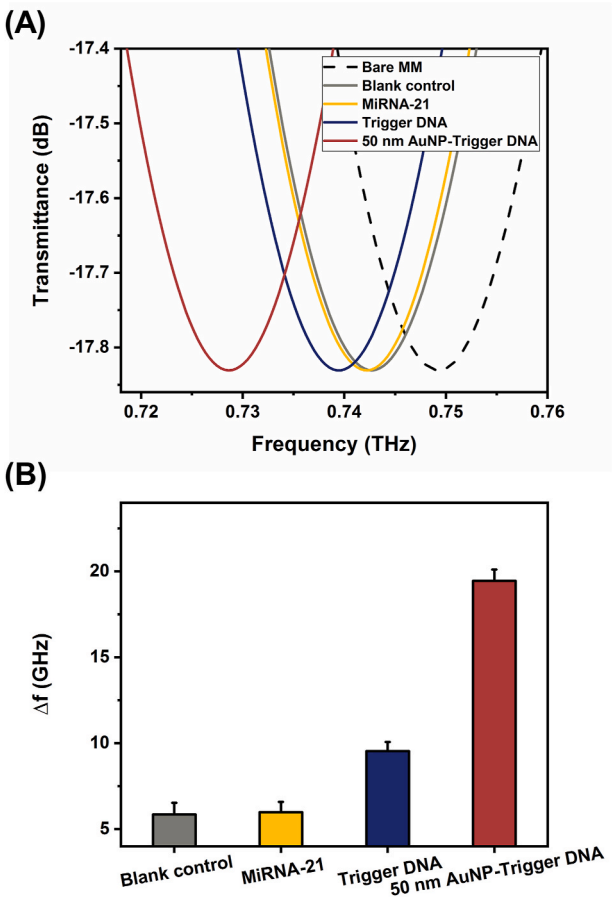

Fig. 4. (A) Normalized THz transmission spectra of bare metamaterial, blank control, miRNA-21 (100 fM), Trigger DNA without AuNPs, and 50 nm AuNP-Trigger DNA complexes. (B) Metamaterial frequency shifts (Δf) of blank control, miRNA-21 (100 fM), Trigger DNA without AuNPs, and 50 nm AuNP-Trigger DNA complexes. One-hundred fM of miRNA-21 was used to obtain the signals from Trigger DNA and 50 nm AuNP-Trigger DNA complexes. DEPC-treated water served as the blank control. Error bars indicate the SD ($n = 3$).

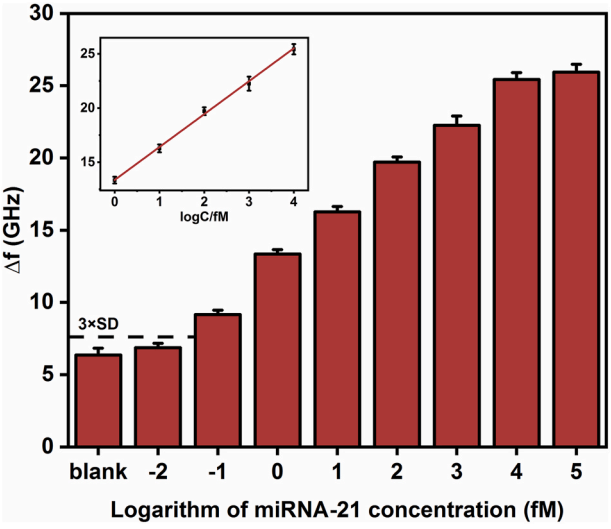

Fig. 5. Sensitivity of THz metamaterial biosensor for miRNA-21 detection. The inset graph shows the linear relationship between Δf and the logarithm of miRNA-21 concentration. Error bars indicate the SD ($n = 3$).

observed between Δf and the logarithm of miRNA-21 concentration over the range from 1 fM to 10 pM. The linear regression equation producing the least squared error is expressed as $\Delta f = 3.04 logc + 13.37 (R^2 = 0.9985)$, and the limit of detection (LOD) is determined to be 14.54 aM. The LOD was calculated from the 3-fold standard deviation (SD) of the blank signal. Compared with other reported biosensors for miRNAs detection, this THz metamaterial biosensor exhibited good analytical performance. As shown in Table S3, the LOD achieved in this work attains attomolar level sensitivity, which is comparable to common opto/electronic biosensors, such as those using the electrochemiluminescence, electrochemical, and photoelectrochemical assays, but exceeds some optical biosensors, such as colorimetric, SERS, and SPR biosensors. Such high sensitivity can mainly be attributed to the design of the metamaterials and the high refractive index of the AuNPs. The four-fold rotationally-symmetric unit cells of the SRRs concentrate the resonant energy in the local gaps by enhancing the electric resonance response and eliminating the magnetic response under the incident THz wave (Xu et al., 2017). In addition, the high refractive index of AuNPs is favorable to enhance THz response (Xu et al., 2016). Compared to other approaches for sensitivity improvement, such as metallic mesh structures, the AuNPs-enhanced metamaterials provide additional advantages of easy accessibility, simple implementation, and low cost.

3.5. Specificity and reproducibility of THz metamaterial biosensor for miRNA-21 detection

To investigate the specificity of THz metamaterial biosensor for miRNA-21 detection, the signals of the target miRNA (miRNA-21), single-base mismatched miRNA-21 (SM), double-base mismatch miRNA-21 (DM), and non-complementary (NC) sequence were compared. In addition, miRNA-25, miRNA-139a, a mixture of miRNA-25 and miRNA-139a samples (Mix A), and a mixture of miRNA-21, miRNA-25 and miRNA-139a samples (Mix B) were also measured. As shown in Fig. 6, the Δf of the target miRNA sample was significantly greater than those of SM, DM, NC, miRNA-25, miRNA-139a and Mix A ($P < 0.05$). In addition, the Δf of Mix B was nearly the same as the value of the target miRNA, demonstrating good specificity for detecting miRNA-21 in the presence of potential interferences. The degree of interference (DI) of the miRNA sample was calculated using equation

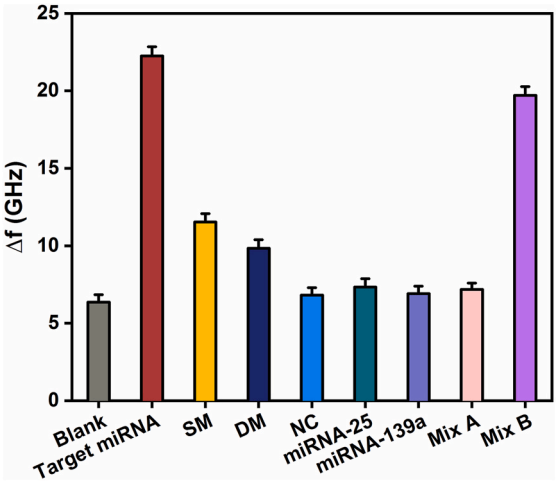

Fig. 6. Specificity of miRNA-21 detection by the THz metamaterial biosensor. SM, DM and NC represent the single-base mismatch miRNA-21, double-base mismatch miRNA-21, and non-complementary sequence, respectively. Mix A is composed of miRNA-25 and miRNA-139a samples with a mixing proportion of 1:1. Mix B is composed of miRNA-21, miRNA-25 and miRNA-139a samples with a mixing proportion of 1:1:1. All the sequence information is given in Table S1. The concentrations of these samples were 1 pM. Error bars indicate the SD (n = 3).

(1). The DI values of the three interfering miRNAs and Mix A were all below 10% (6.17% for miRNA-25, 3.46% for miRNA-139a, and 5.16% for Mix A). The high capacity to resist interferences is very favorable for practical clinical applications, since numerous potential interferences occur in clinical samples. The reproducibility of this biosensor was evaluated using the relative standard deviation (RSD) obtained from five replicate measurements on a 1 pM sample of miRNA-21. The RSDs were calculated to be 2.91%, suggesting that acceptable reproducibility was achieved.

3.6. Clinical sample assay

The application of this THz metamaterial biosensor was practically tested by measuring miRNA-21 in spiked clinical serum samples. Samples spiked with miRNA-21 concentrations of 10 pM, 1 pM, 100 fM, and 10 fM were prepared according to the aforementioned protocol in the SI. As shown in Table S4, the RSD of serum samples ranges from 2.31% to 4.77%, while the recoveries were calculated to be in the range between 90.92% and 107.01%. These results suggest that the complex matrix of interferences in serum samples produces limited perturbations on the miRNA-21 measurements. Therefore, the proposed THz metamaterial biosensor shows satisfactory performance for detection of target miRNA molecules in practical samples. Conventional miRNA detection methods, such as northern blotting, microarrays, and RT-PCR, typically require chemiluminescent, fluorescent, or radioactive probes. Some reagents are toxic or even suspected to be carcinogens (Kilic et al., 2018). The THz biosensor satisfies the requirement for an environmentally safe measurement, which avoids potential biological hazards of chemical labeling reagents. With the aid of the arrayed metamaterial chip in this study, multiple (nine) samples can be loaded simultaneously and serially detected within 10 min. As a result, both convenience of sample preparation and high-throughput measurement can be realized.

4. Conclusion

Our study fabricated a new polarization-independent THz metamaterial biosensor for the highly sensitive detection of miRNA-21, based on the signal augmentation by SDA processing and introduction of metallic nanoparticles. The complexes of miRNA-21 SDA products and nanoparticles exhibited large THz frequency shifts in metamaterials due to the high refractive index of the metallic nanoparticles. Both the experimental and simulated results revealed that 50 nm AuNPs functioned as the optimal nanoparticle size for THz signal enhancement. Based on the dual signal enhancement strategies, our biosensor presented good sensitivity for miRNA-21 detection with an LOD of 14.54 aM. It also demonstrated excellent specificity and was capable of discriminating differences among miRNAs differing by as little as one substituted base. The recoveries of miRNA-21 in spiked clinical serum samples were calculated to be in the range between 90.92% and 107.01%. These findings demonstrate that the novel THz biosensor described herein affords highly sensitive and specific miRNA detection, with noteworthy potential for applications in nucleic acid analysis and cancer diagnosis. The current instrument requires each operation of sample processing be performed independently. This ensures minimum error in carrying out the SDA procedure, but increases the complexity and testing duration at the same time. In future work, coating the chip surface with probes that are complementary to the Trigger DNA are worth pursuing to harvest the SDA products without requiring multiple magnetic fractionation steps. This idea will be tested on the metamaterial chips to see if the speed of sample processing can be hastened from the established timeline without introducing decrements in sensitivity or accuracy. Such conditions will be more favorable for further improving accessibility, speed, and reproducibility, all of which are preferable in practical clinical applications.

CRediT authorship contribution statement

Ke Yang: Conceptualization, Investigation, Writing - original draft, contributed equally to this work. **Jining Li:** contributed equally to this work, Methodology, Software, Formal analysis. **Marc Lamy de la Chapelle:** Writing - review & editing. **Guorong Huang:** Data curation. **Yunxia Wang:** Funding acquisition. **Jinbao Zhang:** Resources. **Degang Xu:** Funding acquisition. **Jianquan Yao:** Writing - review & editing. **Xiang Yang:** Conceptualization, Investigation, Writing - review & editing, Funding acquisition. **Weiling Fu:** Conceptualization, Supervision, Writing - review & editing, Project administration, Funding acquisition.

Declaration of competing interest

The authors declare that they have no known competing financial interests or personal relationships that could have appeared to influence the work reported in this paper.

Acknowledgements

This work was supported by National Natural Science Foundation of China (81920108024, 81802118, 61705162) and the Basic Science and Frontier Technology Research Project of Chong Qing (cstc2017jcyjB0004).

Appendix A. Supplementary data

Supplementary data to this article can be found online at https://doi.org/10.1016/j.bios.2020.112874.

References

Barrera, R.G., Giraldo, J., Mochán, W.L., 1993. Phys. Rev. B 47 (14), 8528–8538.
Cheon, H., Yang, H.-j., Lee, S.-H., Kim, Y.A., Son, J.-H., 2016. Sci. Rep. 6 (1), 37103.
Hasebe, T., Kawabe, S., Matsui, H., Tabata, H., 2012. J. Appl. Phys. 112 (9), 094702.
Kilic, T., Erdem, A., Ozsoz, M., Carrara, S., 2018. Biosens. Bioelectron. 99, 525–546.
Li, T., Wu, X., Tao, G., Yin, H., Zhang, J., Liu, F., Li, N., 2018. Biosens. Bioelectron. 105, 137–142.
Lynch, D.W., Hunter, W.R., 1997. Comments on the optical constants of metals and an introduction to the data for several metals. In: Handbook of Optical Constants of Solids. Sachs/Freeman Associates, Inc., Bowie, Maryland, pp. 275–367.
Niessen, K.A., Xu, M., George, D.K., Chen, M.C., Ferré-D'Amaré, A.R., Snell, E.H., Cody, V., Pace, J., Schmidt, M., Markelz, A.G., 2019. Nat. Commun. 10 (1), 1–10.
Park, S.J., Jun, S.W., Kim, A.R., Ahn, Y.H., 2015. Opt. Mater. Express 5 (10), 2150–2155.
Park, S.J., Son, B.H., Choi, S.J., Kim, H.S., Ahn, Y.H., 2014. Optic Express 22 (25), 30467–30472.
Qin, J., Xie, L., Ying, Y., 2016. Food Chem. 211, 300–305.
Tang, M., Huang, Q., Wei, D., Zhao, G., Chang, T., Kou, K., Wang, M., Du, C., Fu, W.-l., Cui, H.-L., 2015. J. Biomed. Optic. 20 (9), 095009.
Tang, S., Gu, Y., Lu, H., Dong, H., Zhang, K., Dai, W., Meng, X., Yang, F., Zhang, X., 2018. Anal. Chim. Acta 1004, 1–9.
Xu, W., Xie, L., Ying, Y., 2017. Nanoscale 9 (37), 13864–13878.
Xu, W., Xie, L., Zhu, J., Xu, X., Ye, Z., Wang, C., Ma, Y., Ying, Y., 2016. ACS Photonics 3 (12), 2308–2314.
Xue, T., Liang, W., Li, Y., Sun, Y., Xiang, Y., Zhang, Y., Dai, Z., Duo, Y., Wu, L., Qi, K., Shivananju, B.N., Zhang, L., Cui, X., Zhang, H., Bao, Q., 2019. Nat. Commun. 10 (1), 1–9.
Yang, X., Yang, K., Zhao, X., Lin, Z., Liu, Z., Luo, S., Zhang, Y., Wang, Y., Fu, W., 2017. Analyst 142 (24), 4661–4669.
Yin, H.S., Li, B.C., Zhou, Y.L., Wang, H.Y., Wang, M.H., Ai, S.Y., 2017. Biosens. Bioelectron. 96, 106–112.